H–H and C–H Activation Reactions at d^0 Metal Centers

H. Rabaâ,[†] J.-Y. Saillard,*[†] and R. Hoffmann*[‡]

Contribution from the Laboratoire de Chimie du Solide et Inorganique Molêculaire, U.A. 254, Université de Rennes I, Campus de Beaulieu, 35042 Rennes, Cedex, France, and the Department of Chemistry, Cornell University, Ithaca, New York 19853. *Received October 22, 1985*

Abstract: An extended Hückel MO analysis of H–H and C–H activation reactions by d^0 ML_n species, such as Cp_2LuR, is reported. Two mechanisms are considered. The first mechanism involves a transition state with an electron-deficient coordination mode. The second mechanism involves an envisaged reaction intermediate, in which the σ bond is oxidatively added, the oxidation taking place at the Cp's. The second mechanism is less likely for the systems considered because of a high 2-fold energy barrier associated with the oxidative addition/reductive elimination process. The electronic structure of the reaction intermediate in the first mechanism is considered in detail, and other related reactions are analyzed.

Progress in the exciting field of activation of σ bonds (H–H or C–H) has been rapid.[1,2] These bond-breaking reactions occur generally via an oxidative addition process **1**.[3] The σ H–R bond

$(M = d^n)$ $(M = d^{n-2})$

$(R = H, CR'_3 \ldots)$

1

interacts typically with an unsaturated ML_n reactive species to give a generally saturated compound where the oxidized metal is bonded to the formally two-electron ligands, H^- and R^-. In this kind of reaction the number of metal d electrons in the ML_n reactive species must be at least $n = 2$. However, there is a class of H–H and C–H activation reactions in which the metal is d^0 in the starting ML_n species.[4] This kind of reaction occurs generally with organolanthanide,[5] organoactinide,[6] or early transition-metal complexes.[5a,7] A general formulation for these reactions is given in **2**. A typical example is Watson's methane exchange reaction[5a,b] shown in **3**.

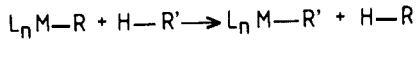

$M = d^0$

$(R, R' = H, CH_3 \ldots)$

2

$M = Lu, Y$

$Cp = \eta^5\text{-}C_5Me_5$

3

This paper deals with selected theoretical aspects in this class of H–H and C–H (alkane) reactions.

C–H and H–H Activation by Lutetium Methyl and Lutetium Hydride Complexes. From kinetic studies[5a] it has been suggested that reaction 3 occurs through a symmetrical transition state **4**. Since the metal atom is d^0 (Lu^{III}) in $Cp_2'LuCh_3$, if there were an oxidative addition of CH_4 to that metal, one might think that 4f electrons are involved. But the 4f electrons of Lu, lying at low energy, are hardly available; moreover, reaction 3 works also

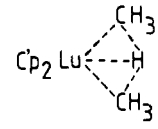

4

with M = Y,[5a] which has no f electrons. In the latter case, if there were oxidation, it should occur at the ligands (we shall discuss

[†] Université de Rennes I.
[‡] Cornell University.

(1) See for example (and referencs therein): Collman, J. P.; Hegedus, L. S. *Principles and Applications of Organotransition Metal Chemistry*; University Science Books: Mill Valley, CA, 1980. James, B. R. *Homogeneous Hydrogenation*; Wiley: New York, 1973. Webster, D. E. *Adv. Organomet. Chem.* **1977**, *15*, 147. Parshall, G. W. *Acc. Chem. Res.* **1970**, *3*, 139; *Chem. Technol.* **1974**, *4*, 445; *Acc. Chem. Res.* **1975**, *8*, 113; *Catalysis* **1977**, *1*, 335. Muetterties, E. L. *Chem. Soc. Rev.* **1982**, *11*, 283. Halpern, J. *Discuss. Faraday Soc.* **1968**, *46*, 7; *Acc. Chem. Res.* **1970**, *3*, 386. Shilov, A. E.; Shteinman, A. A. *Coord. Chem. Rev.* **1977**, *24*, 97. Shilov, A. E. *Activation of Saturated Hydrocarbons by Transition Metal Complexes*; D. Reidel: Dordrecht, Boston, Lancaster, 1984.

(2) Theoretical treatments on related problems: (a) Dedieu, A.; Strich, A. *Inorg. Chem.* **1979**, *18*, 2940. (b) Sevin, A. *Nouv. J. Chim.* **1981**, *5*, 233. (c) Saillard, J. Y.; Hoffmann, R. *J. Am. Chem. Soc.* **1984**, *106*, 2006. (d) Goddard, R. J.; Hoffmann, R.; Jemmis, E. D. *J. Am. Chem. Soc.* **1980**, *102*, 7667. (e) Eisenstein, O.; Jean, Y. *J. Am. Chem. Soc.* **1985**, *107*, 1177. (f) Kitaura, K.; Obara, S.; Morokuma, K. *J. Am. Chem. Soc.* **1985**, *103*, 2891. (g) Brintzinger, H. H. *J. Organomet. Chem.* **1979**, *171*, 337. (h) Koga, N.; Shigeru, O.; Morokuma, K. *J. Am. Chem. Soc.* **1984**, *106*, 4625; *J. Organomet. Chem.* **1984**, *270*, C33. (i) Noell, J. O.; Hay, P. J. *J. Am. Chem. Soc.* **1982**, *104*, 4578. (j) Low, J. J.; Goddard, W. A., III. *J. Am. Chem. Soc.* **1984**, *106*, 6228. (k) Fitzpatrick, N. J.; McGinn, M. A. *J. Chem. Soc., Dalton Trans.* **1985**, *8*, 1637.

(3) Vaska, L. *J. Am. Chem. Soc.* **1966**, *88*, 4100. Vaska, L.; Catone, D. L. *J. Am. Chem. Soc.* **1966**, *88*, 5324. Longato, B.; Morandini, F.; Bredasola, S. *Inorg. Chem.* **1976**, *15*, 650. Drouin, M.; Harrod, J. F. *Inorg. Chem.* **1983**, *22*, 999. Johnson, C. J.; Fisher, B. J.; Eisenberg, R. *J. Am. Chem. Soc.* **1983**, *105*, 7772. Fisher, B. J.; Eisenberg, R. *Organometallics* **1983**, *2*, 764. Jones, W. D.; Feher, F. J. *J. Am. Chem. Soc.* **1982**, *104*, 4240. Jones, W. D.; Feher, F. J. *J. Am. Chem. Soc.* **1984**, *106*, 1650. Jones, W. D.; Feher, F. J. *J. Am. Chem. Soc.* **1985**, *107*, 620. Crabtree, R. H.; Khan, H. F. T.; Morris, G. E. *J. Organomet. Chem.* **1977**, *141*, 205. Crabtree, R. H.; Quirk, J. M.; Khan, H. F. T.; Morris, G. E. *J. Organomet. Chem.* **1978**, *157*, C13. Crabtree, R. H.; Khan, H. F. T.; Morris, G. E. *J. Organomet. Chem.* **1979**, *168*, 183. Crabtree, R. H. *Acc. Chem. Res.* **1979**, *12*, 331. Crabtree, R. H.; Mihelcic, J. M.; Quirk, J. M. *J. Am. Chem. Soc.* **1979**, *101*, 7738. Crabtree, R. H.; Mellea, M. F.; Mihelcic, J. M. *J. Am. Chem. Soc.* **1982**, *104*, 107. Crabtree, R. H.; Parnell, C. P. *Organometallics* **1984**, *3*, 1727. Burk, M. J.; Crabtree, R. H.; Parnell, C. P.; Uriarte, R. J. *Organometallics* **1984**, *3*, 817. Janowicz, A. H.; Bergman, R. G. *J. Am. Chem. Soc.* **1983**, *105*, 3929. Periana, R. A.; Bergman, R. G. *Organometallics* **1984**, *3*, 508. Wax, M. J.; Stryku, J. M.; Buchanan, M.; Kovac, C. A.; Bergman, R. G. *J. Am. Chem. Soc.* **1984**, *106*, 1121. Periana, R. A.; Bergman, R. G. *J. Am. Chem. Soc.* **1984**, *106*, 7272. Hoyano, K. J.; Graham, W. A. G. *J. Am. Chem. Soc.* **1982**, *104*, 3723. Sweet, J. R.; Graham, W. A. G. *Organometallics* **1983**, *2*, 135. Hoyano, K. J.; McMastmer, A. D.; Graham, W. A. G. *J. Am. Chem. Soc.* **1983**, *105*, 7190. Kletzin, V. H.; Werner, H. *Angew Chem.* **1983**, *95*, 916. Baudry, D.; Ephritikine, M.; Felkin, H. *J. Chem. Soc., Chem. Commun.* **1980**, 1243; **1982**, 606. Baudry, D.; Ephritikine, M.; Felkin, M.; Zakrzeuski, J. *J. Chem. Soc., Chem. Commun.* **1982**, 1235.

(4) For an interesting review on C–H activation in early transition-metal systems, see: Rothwell, I. P. *Polyhedron* **1985**, *4*, 177.

0002-7863/86/1508-4327$01.50/0

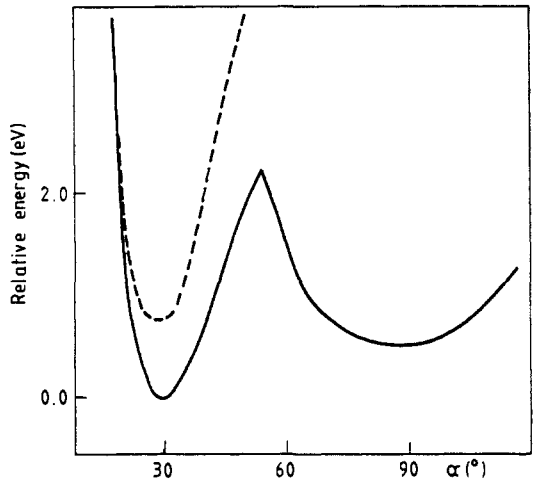

Figure 1. Total energy of compounds **6** (solid line) and **7** (dashed line) with respect of the angle α. The common energy zero for both curves is the energy of the deepest minimum.

this point later). For these reasons an electron-deficient coordination mode (i.e. four-electron, four-center bonding) appears more probable for **4**. This kind of transition state, with such an electron-deficient coordination mode, has also been suggested for other reactions of type 2.[2f,4-7]

Taking advantage of the isolobal analogy of CH_3 and H, we first studied reaction 5, a simplified model for reaction 3, where the prime symbol is used only to differentiate the H atoms. Note that this reaction is not so hypothetical, for it has been shown to occur with H′≡D and methylated Cp's.[5c]

$$Cp_2LuH + H'_2 \longrightarrow Cp_2LuH' + HH'$$

5

Our first goal was to optimize the geometry of the supposed symmetrical transition state Cp_2LuHH_2'. Two conformations, **6** and **7**, have been considered: in **6** the three H's are in the plane

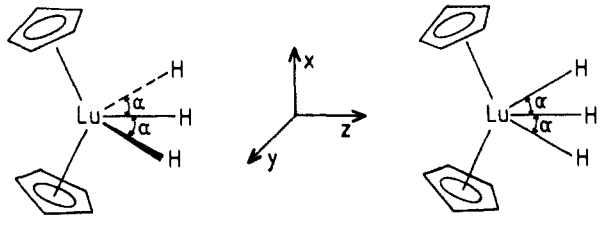

6 **7**

between the Cp rings; in **7** two H's lie above and below that plane. For both conformations, the geometry of the bent Cp_2Lu fragment was kept identical; the distances and angles were chosen from representative experimental Cp_2Ln complexes (see Appendix). The Lu–H bond distances were first fixed at 2.1 Å.

The variation of the total energy of **6** and **7** with respect to α is shown in Figure 1. From this figure it is clear that conformation

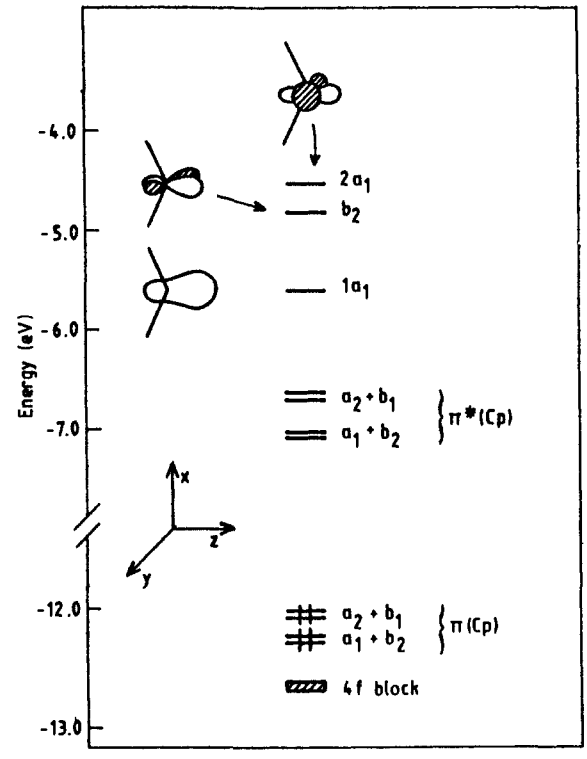

Figure 2. Highest occupied and lowest unoccupied MOs of the bent Cp_2Lu^+ fragment.

7 is unfavorable. The reasons for this are part steric, part electronic. At large α the H's are too close to the Cp's; at small α they are too close to each other. The overlap with Cp_2Lu orbitals is also not optimal in this plane, for as we will see below the valence orbitals of Cp_2Lu extend in the plane between the Cp rings. Therefore, we will concentrate the discussion on conformation **6**.

Figure 1 presents two minima for **6**, separated by an energy barrier of ~2 eV. The lower minimum, at $\alpha = 30°$, corresponds to H···H distances of 1.09 Å; the secondary minimum, at $\alpha = 90°$, lies 0.5 eV higher and corresponds to H···H separations of 2.97 Å. The variation of the total energy with respect to α was also calculated for Lu–H distances of 2.3 and 1.9 Å. It leads to curves very similar to the ones depicted in Figure 1; the main difference is only a shifting (up and down, respectively) of the curves in energy.

Both geometries, **6** ($\alpha = 30°$) and **6** ($\alpha = 90°$), can be described as a system of three H atoms interacting with a Cp_2Lu fragment. Because these geometries will turn out to be important in the sequel and are electronically different, we will provide them with different labels, and a better drawing, in **8** and **9**. Before entering upon

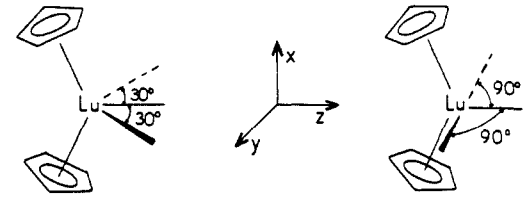

8 **9**

an orbital analysis of these two geometries, let us recall briefly the MO picture of the bent Cp_2Lu fragment,**8** which is represented on Figure 2 with an orbital occupation corresponding to Lu^{III}, $4f^{14}$ $5d^0$, namely Cp_2Lu^+. This fragment possesses three high-lying empty frontier orbitals: $1a_1$, mainly *s*, *z*, and z^2 in character; $1b_2$ mainly *yz* and *y*; and $2a_1$, mainly y^2-z^2. The spatial representation

(5) (a) Watson, P. L. *J. Am. Chem. Soc.* **1983**, *105*, 6491. (b) Watson, P. J.; Parshall, G. W. *Acc. Chem. Res.* **1985**, *18*, 51. (c) Watson, P. L. *J. Chem. Soc., Chem. Commun.* **1983**, 276.

(6) Fagan, P. J.; Manriquez, J. M.; Maota, E. A.; Seyan, A. M.; Marks, T. J. *J. Am. Chem. Soc.* **1981**, *103*, 6650. Bruno, J. W.; Marks, T. J. *J. Am. Chem. Soc.* **1982**, *104*, 7357. Marks, T. J. *Science (Washington, D.C.)* **1982**, *217*, 989. Manermann, H.; Sweptson, P. N.; Marks, T. J. *Organometallics* **1985**, *4*, 200. Jeske, G.; Lauke, H.; Manermann, H.; Schumann, H.; Marks, T. J. *J. Am. Chem. Soc.* **1985**, *107*, 811.

(7) McAlister, D. R.; Erwin, D. K.; Bercaw, J. E. *J. Am. Chem. Soc.* **1978**, *100*, 5966. Mayer, J. M.; Bercaw, J. E. *J. Am. Chem. Soc.* **1982**, *104*, 2157. Gell, K. I.; Schwartz, J. *J. Am. Chem. Soc.* **1978**, *100*, 3246. Gell, K. I.; Posin, B.; Schwartz, J.; Williams, M. *J. Am. Chem. Soc.* **1982**, *104*, 1846. Chiu, K. W.; Jones, R. A.; Wilkinson, G.; Galas, A. M. R.; Hursthouse, M. B.; Abdul-Malik, K. M. *J. Chem. Soc., Dalton Trans.* **1981**, *5*, 1204.

(8) For a detailed MO analysis of Cp_2M and Cp_2Ln fragments see: (a) Lauher, J. W.; Hoffmann, R. *J. Am. Chem. Soc.* **1976**, *98*, 1729. (b) Ortiz, J. V.; Hoffmann, R. *Inorg. Chem.* **1985**, *24*, 2095.

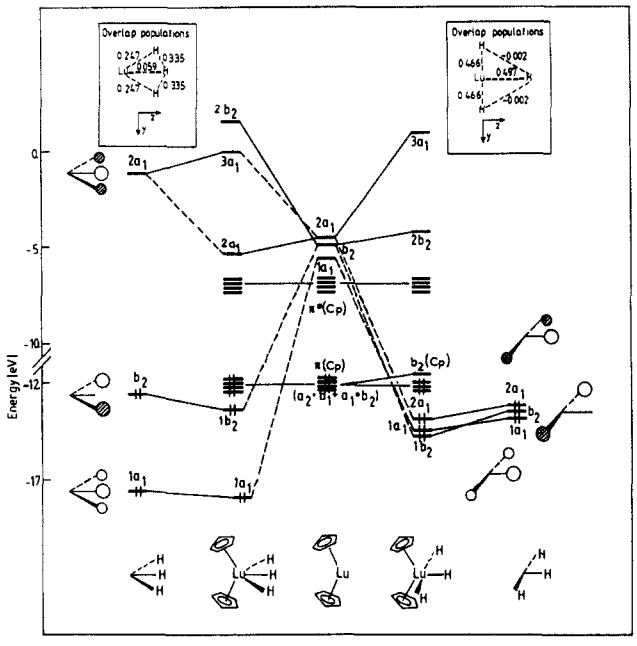

Figure 3. Interaction diagrams for H_3 and Cp_2Lu: left, compound **8** (α = 30°); right, compound **9** (α = 90°).

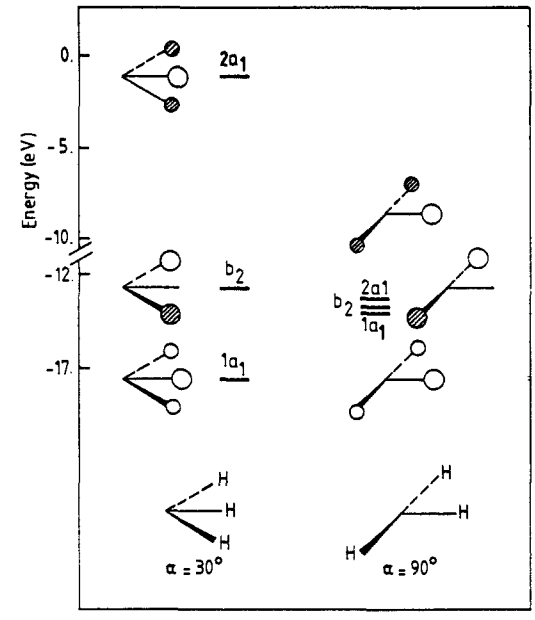

Figure 4. MOs of the H_3 fragment: left in compound **8** (α = 30°, H···H = 1.09 Å); right in compound **9** (α = 90°, H···H = 2.97 Å).

of $1a_1$ and $2a_1$ is approximate but suggestive of their different shape.

These three fragment molecular orbitals (FMOs) lie above a block of four empty orbitals derived from the $\pi^*(e'')$ orbitals of the two Cp's. The highest occupied orbital set is a block of four MOs derived from the $\pi(e')$ orbitals of the Cp's. Note that these π(Cp) MOs lie above the seven Lu 4f orbitals which are almost nonbonding. Actually, for all the calculations we did on Cp_2Lu complexes, these contracted that 4f orbitals remain nonbonding, thus allowing us to omit them in most of our calculations (see Appendix).

Similar calculations on the $4f^5\ 5d^0$ Cp_2Sm fragment found the 4f block lying above the π(Cp) MOs. It is likely that this result can be extended to most of the stable d^0 Cp_2Ln complexes in which the 4f electron count is less than 14.

MO Picture of 8. On the left side of Figure 3 is the interaction diagram for **8**. The FMO set of the H_3 fragment represented on the left side of Figure 4 is particularly simple: two orbitals of a_1 symmetry (with respect to the C_{2v} symmetry group of the complex) and one of b_2 symmetry. At the H···H separation of 1.09 Å corresponding to α = 30°, the H_3 FMO $1a_1$ is strongly bonding and lies at low energy. On the other hand, the antibonding $2a_1$ FMO is very much destabilized. The energy of the mainly nonbonding b_2 FMO is not very different from the energy of an isolated hydrogen 1s AO.

For reasons of matching spatial extension and consequent good overlap, $1a_1$ of the H_3 fragment interacts mainly with $1a_1$ of the Lu fragment, while $2a_1$ of the H_3 fragment interacts primarily (and to a moderate extent) with $2a_1$ of the other fragment. Finally the two b_2 FMOs interact strongly. The resulting orbital picture of **8** is the following: MOs $1a_1$ and b_2 of the H_3 fragment are stabilized, respectively, by FMOs $1a_1$ and b_2 of $LuCp_2$. They then generate two occupied MOs. The interaction between the $2a_1$ levels has no effect on the bonding, since they generate two unoccupied MOs.

The coordination mode in **8** can be formally viewed as an H_3^- ligand coordinated to a Cp_2Lu^+ fragment,[6] the four electrons of H_3^- being delocalized over four centers (the three H atoms and the Lu atom). This is consistent with previously cited suggestions[4-7] and MO calculations on related Zr^{IV} systems by Brintzinger.[2g].

Of the two bonding interactions, the b_2 one is the strongest because the two interacting FMOs are closer in energy. This is consistent with the FMO population analysis in the complex which gives, respectively, 1.67 and 1.92 electrons in the b_2 and $1a_1$ FMOs of H_3^-. It is also consistent with the overlap population analysis (insert, left side of Figure 3) which shows less bonding between lutetium and the central H atom. The H(central)–Lu distance is therefore expected to be larger. As extended Hückel calculations are not suitable for a full optimization of bond distances, we did the following partial optimization: keeping the H···H separation constant and equal to 1.09 Å, both types of Lu–H distances were allowed to vary prioviding their average remained constant and equal to 2.1 Å. Surprisingly, the energy minimum was found for a shorter Lu–H(central) distance (2.0 vs. 2.15 Å for the two others). The reason is that the dominant b_2 interaction imposes, for a given H···H separation, a rather large H(side)–Lu–H(side) angle and therefore a large H···H···H angle and consequently a rather short central H–Lu distance.

MO Picture of 9: The Other Minimum. The level interaction diagram of **9** is presented on the right side of Figure 3. The FMOs of the H fragment have of course the same phase relationship as for α = 30° (see Figure 4 right), but now the H atoms are far from each other and those three FMOs are all nonbonding, lying at the energy of an isolated 1s level for the hydrogen atom.

As for α = 30° there is a similar one-to-one interaction between the MOs of Cp_2Lu and of the H fragment. This time the three H_3 FMOs are at lower energy than those of the metal fragment. They are consequently stabilized, generating in the complex three occupied MOs $1a_1$, b_2, and $2a_1$. The coordination mode can be viewed as that of three H^- ligands bonded to a Cp_2Lu^{3+} fragment. If that is so, that is, if H_2 is reduced to 2 H^- in the process, and three mainly hydride MOs are occupied, where do the electrons needed for the reduction come from? In our calculations they come not from the Lu f orbitals but from the π(Cp) block. Four nearly degenerate Cp π orbitals may be seen in Figures 2 and 3. One of these (of b_2 symmetry) is emptied and its electrons are transferred to H_2.

There are several consequences of this highly unusual Cp ligand oxidation. (i) The π(Cp) block is Lu–Cp bonding. The creation of a hole in that block should weaken the Lu–Cp bonding and possibly make that bonding unsymmetrical (different Lu–C distance). (ii) The π(Cp) b_2 orbital has some Lu character. Consequently it interacts with the H_3 b_2 FMO and is destabilized with respect to the other π(Cp) levels. (iii) The resulting HOMO–LUMO gap in **9** is only 0.15 eV. One might anticipate a triplet ground state for this hypothetical intermediate, or a Jahn-Teller distortion described in (i) may occur to give a singlet species.

Given the approximate nature of our method, the significance of the calculated 0.5-eV energy difference between **8** and **9** is

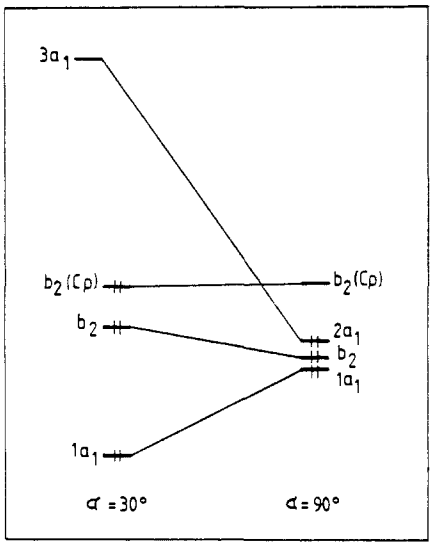

Figure 5. Schematice evolution of the crucial energy levels during the 8 → 9 transit. Levels not playing an important role (and consequently some avoided crossings) have been omitted.

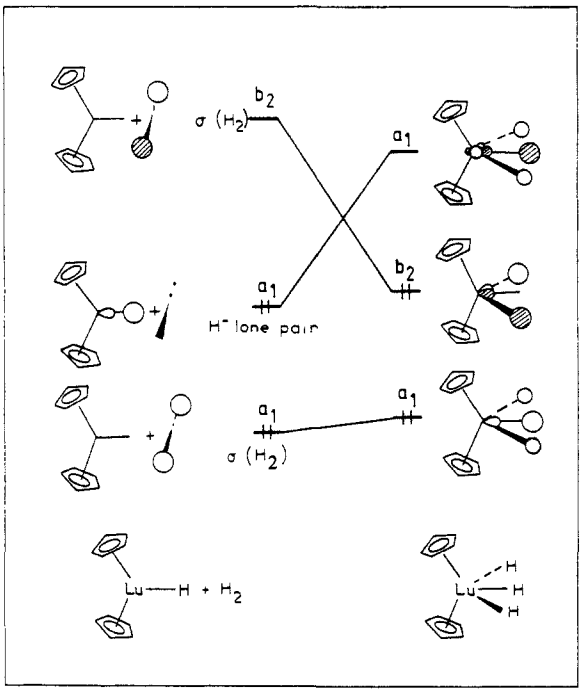

Figure 6. Schematic evolution of the levels preponderantly of hydrogen character during the symmetry-forbidden process 10.

questionable. The possibility that the transition state or intermediate of reaction 5 is an oxidatively added species is not excluded a priori. We undertook the study of reaction 5 assuming either **8** or **9** to be a way point along the reaction coordinate. But before that, let us interpret the energy barrier associated with the **8** → **9** transit.

Origin of the Energy Barrier during the 8 → 9 Transit. Figure 5 shows the level correlation diagram of **8** ⇄ **9**. This diagram is schematic, indicating essential intended correlations, which in a real correlation diagram might be transformed into unimportant avoided crossings by intervening levels of the same symmetry. The main features of the correlation diagram are a strong stabilization of the highest (antibonding) H level, $2a_1$, and a significant destabilization of $1a_1$ during the transit. A HOMO–LUMO level crossing occurs, corresponding to the transfer of two electrons from the Cp's to the H system. This is responsible for the energy cusp in Figure 1. Before the level crossing, the energy of the HOMO is constant, and the total energy variation follows the destabilization of the $1a_1$ level. After the level crossing, the total energy

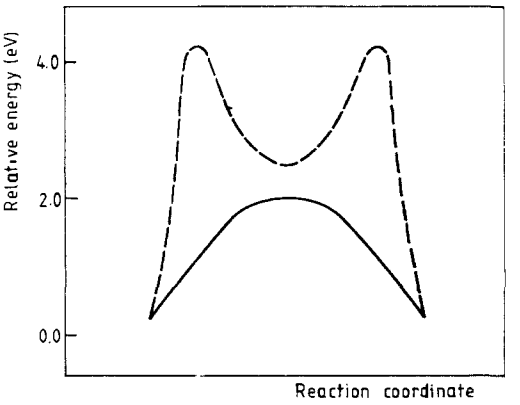

Figure 7. Computed potential energy curves of reaction 11 for hypothetical reaction coordinates, assuming the midpoint of the reaction is **8** (solid line) or **9** (dashed line).

variation is driven by the stabilization of the hydrogen antibonding HOMO.

Path of Reaction 5. We first investigated reaction 5 assuming **8** as the midpoint of the reaction coordinate. Hypothetical reaction coordinates were constructed, assuming a linear transit between the starting point (Cp_2LuH interacting weakly with H_2' (Lu···H' = 2.6 Å; H'–H' = 0.74 Å)) and the midpoint. The second portion of the transit was defined in the same way.

The symmetrical approach 10 was examined first. A huge energy barrier was encountered, due to a level crossing of hydrogen orbitals, as indicated schematically in Figure 6.

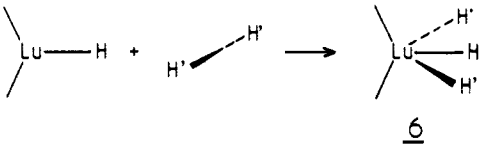

6

10

The lower symmetry process 11 was then considered. To prevent steric hindrance with the approaching H_2' molecule, the starting Cp_2LuH complex was bent and the H moved off the 2-fold axis. This bending of 30° does not change significantly the energy

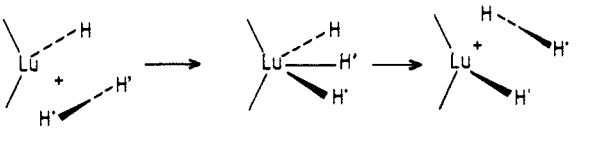

11

of Cp_2LuH. The variation of the total energy of the system during this transit is shown in Figure 7 (solid line). This curve is symmetric with respect to the midpoint **8** which is the highest energy point. Indeed, **8** is the transition state of the reaction. The height of the energy barrier is probably overestimated, due to the overestimation of H–H bonding with resepct to metal–H bonding at the extended Hückel level. We then investigated reaction 5 assuming that **9** is the midpoint of a reaction process identical with 11. The variation of the total energy during the transit is also represented in Figure 7 (dashed line). This time we have an energy barrier before (and after) reaching the midpont **8**. This barrier has the same origin as the one corresponding to the **8** → **9** process, a level crossing due to oxidative addition of H_2'. The starting system of reaction 5 ($Cp_2LuH + H_2'$) has a set of H levels similar to the one of **8**: a low-lying occupied $\sigma_{H_2'}$ MO, a high-lying empty $\sigma^*_{H_2'}$ MO, and a metal-stabilized H^- lone pair level. The second energy barrier corresponds to the symmetrical H–H' reductive elimination process.

The process 11 was also investigated using Sm^{III} in place of Lu^{III}, assuming **9** to be the midpoint of the reaction. The corresponding energy curve was found to be similar to the one of Figure 7 (dashed line). The only difference with the Lu case is

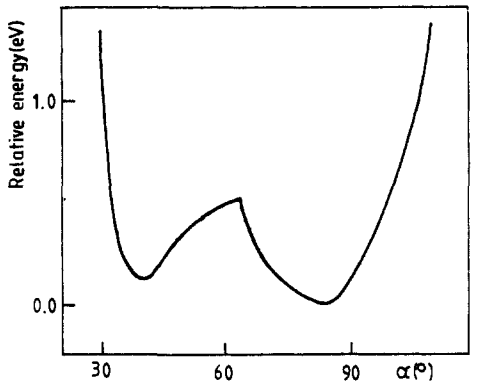

Figure 8. Total energy of compound **12** with respect of the angle α (β = 0°). The energy zero is the energy of the deepest minimum.

that the oxidative addition/reductive elimination process does not involve the b_2 π(Cp) MO of the Cp_2Ln fragment but one of the occupied Sm 4f orbitals, which successively loses and gets back its two electrons with no significant change in energy.

This high 2-fold barrier of Figure 7 allows us to exclude definitely the possibility of an oxidative addition/reductive elimination mechanism for reaction **5** and to conclude that the real mechanism occurs via the electron-deficient transition state **8**. In fact, this reaction can be viewed as the reaction $H^- + H_2 \rightarrow (H_3^-)^* \rightarrow H_2 + H^-$ taking place in the coordination sphere of the Lu^{III} atom.

Methane-Exchange Reaction 3. Reaction 3 was then investigated, using Cp's in place of methylated Cp's. Assuming first a value of 0° for the β angle of the symmetrical intermediate **12**, the α angle was optimized. The results are very similar to those found for **6**. Two energy minima are found (Figure 8): one, at α = 40°, corresponds to an $(H_3CHCH_3)^-$ ligand coordinated to a Cp_2Lu^+ fragment (with H···C = 1.67 Å); the other, at α = 85°,

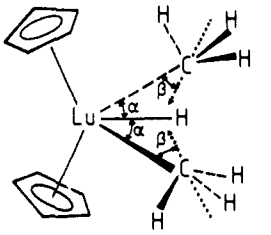

12

corresponds to an oxidatively added C–H bond, with oxidation at the Cp's. These are drawn in **13** and **14**.

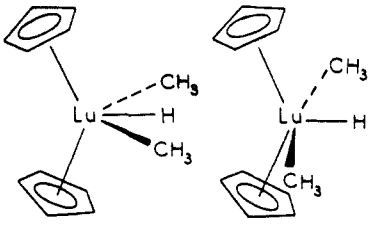

13 **14**

If β is also allowed to vary, the energy minimum **13** at α = 40° becomes the principal minimum, with β = 43°. This significant reorientation of the methyl groups affords a stabilization of 0.8 eV, due to a better bonding within the $(H_3CHCH_3)^-$ ligand and a diminution of steric interactions. The MO interaction diagrams corresponding to these two energy minima of **12** (**13** and **14**) are shown in Figure 9. The similarity to the MO diagram of **8** and **9** is evident.

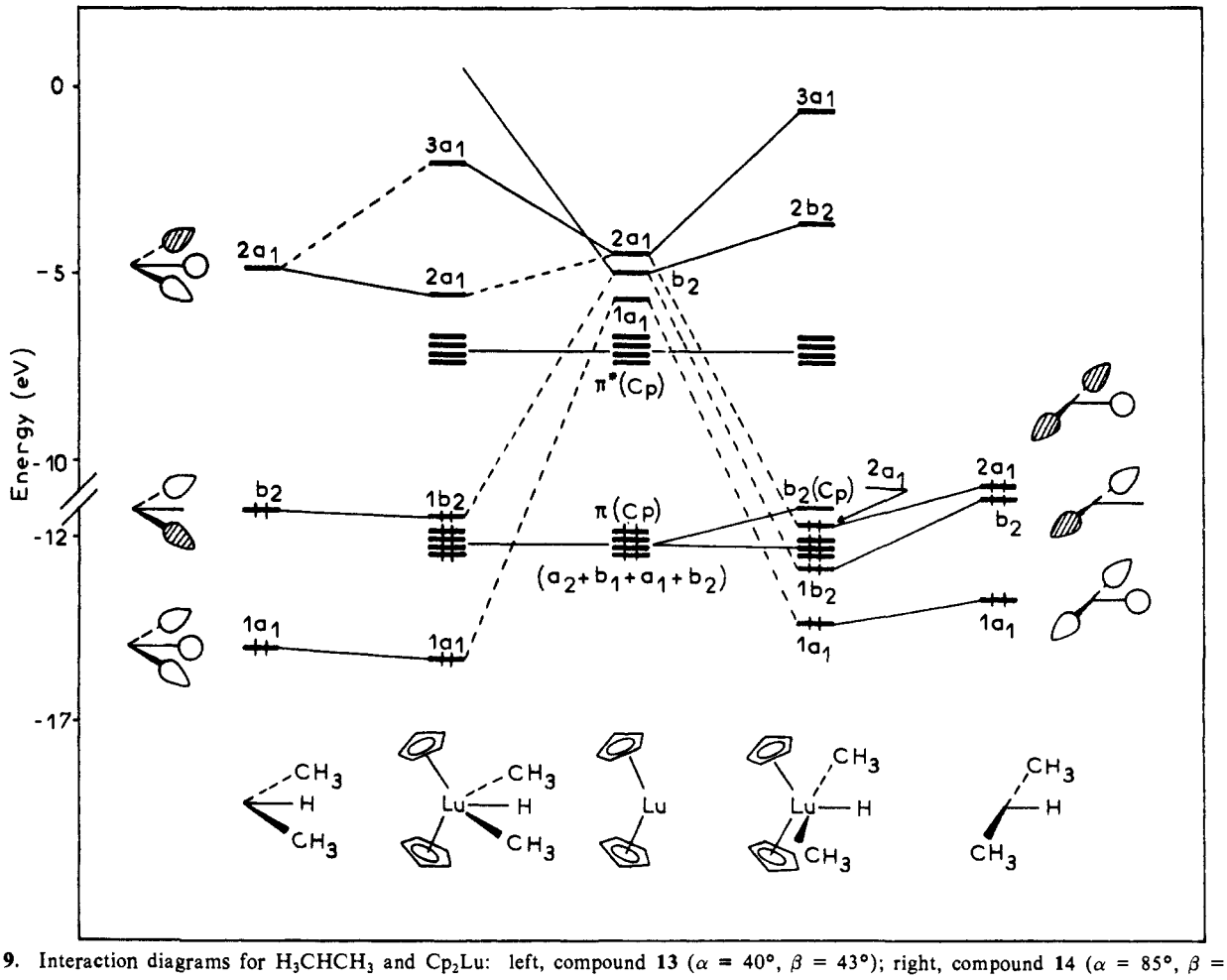

Figure 9. Interaction diagrams for H_3CHCH_3 and Cp_2Lu: left, compound **13** (α = 40°, β = 43°); right, compound **14** (α = 85°, β = 0°).

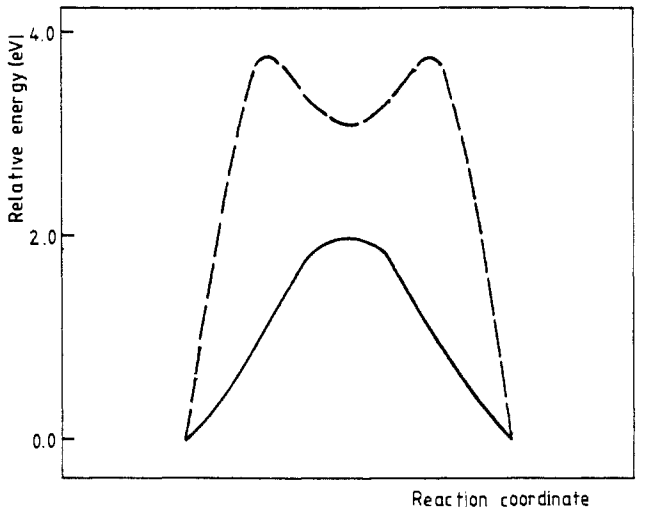

Figure 10. Computed potential energy curve for hypothetical reaction coordinates of the methane-exchange reaction 3 (using Cp's in place of methylated Cp's), assuming the midpoint of the reaction is **13** (solid line) or **14** (dashed line).

The path of the methane-exchange reaction was investigated in the same way as for reaction 5, assuming **13** is the midpoint of the reaction. The variation of the total energy of the system during the two possible transits is shown in Figure 10. As for reaction 5, the process involving the intermediate **14** leads to an unfavorable 2-fold energy barrier corresponding to a double-level crossing associated with the oxidative addition/reductive elimination of a C–H bond to the Cp_2Lu fragment. As for reaction 5, the most favorable path is via a four-center, four-electron transition state, **13**.

Activation of σ Bonds by d^0 Cp_2MR_2 and Cp_2MR_3 Complexes. Reaction 2 occurs also with $Cp_2'MR'_2$ (R' = alkyl, alkoxide, hydride). This kind of reaction is well-known for d^0 Zr^{IV}, U^{IV}, and Th^{IV} complexes.[4-7] A four-center, four-electron transition state has been suggested for these reactions by previous extended Hückel calculations[2g] and other experimental studies.[4-7]

Consistently, our calculations on the model reaction 15 suggest that the most probable reaction path is the same as for reaction 5, with an electron-deficient transition state corresponding to an H_3^- ligand coordianted to a d^0 Cp_2LuH metallic fragment. The possibility of an intermediate resulting from an oxidatively added H_2 molecule is this time excluded.

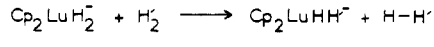

15

Cp_2MH_3 (M = Ta, Nb) complexes has been shown to activate C–H and Si–H bonds.[9] The mechanism of this reaction is necessarily different from those previously discussed in this paper since a stable d^0 Cp_2MH_3 species has no acceptor frontier orbital to stabilize an incoming σ bond in the transition state. The three FMOs of Cp_2M^{3+} are used up in stabilizing the three H^- lone pairs; note that this stable species has the same electronic structure as **6** but with two more electrons. Its optimum geometry has $\alpha \sim 60°$.

Indeed, it is suggested that the active species in these reactions is Cp_2MH, obtained by reductive elimination of H_2.[9] With such a d^2 complex, the σ bond activation reaction proceeds by an oxidative addition of type 1.

Other Related Reactions and Concluding Remarks. For a facile reacton of type 1 the reactive ML_n species must have an empty σ-type MO and a high-energy π-type MO containing the lone pair which will be transferred into the σ^* orbital of the H–R bond during the oxidative addition reaction.[2a-c]

On the other hand, for a reaction of type 2 the reactive species need only have empty acceptor MOs, at least one, to stabilize the entering σ bond electron pair in the transition state. This condition can be achieved for d^0 L_nM–R compounds having $n < 7$, such as Cp_2M–R ($n = 6$) or Cp_2MRR' ($n = 7$), i.e., where the metal has a total coordination number lower than 9 (with a coordination number of 9, all the valence metallic AOs are utilized for metal–ligand bonding and there is no nonbonding metal MO available, as in Cp_2NbH_3). Intramolecular CH oxidative addition reactions of type 1, such as orthometalation, are well-known.[10] Similarly, intramolecular reactions of cyclometalation 16, proceeding by abstraction of distal, α-, β-, or even γ-hydride may be viewed as being of type 2.[4,11] Such an intramolecular mechanism, involving a methyl group of the Cp's, has been also suggested in reaction 3 to compete with the intermolecular reaction path 11.[5b]

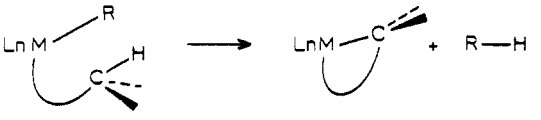

16

For these activation reactions, a mechanism involving a transition state with a multicenter, electron-deficient coordination mode is also often suggested.[4] Consistently, in all of these reactions the total coordination number of the metal atom is lower than 9 ($n < 6$), with various L ligands, allowing it to provide in the transition state at least one empty FMO for interaction with the entering C–H bond.

Finally, reaction 2 has been compared with hydrogenolysis reactions of main group alkyl compounds such as LiR, MgR_2, ZnR_2, AlR_3, etc.[6a] Indeed, it has been suggested that these reactions occur via a MCHH multicenter transition state.[12] This is consistent with the electrophilicity of these alkyl compounds, i.e., that they bear accepting low-lying empty FMOs. Actually, using the isolobal analogy from the starting point of a 9-coordinate, 18-electron metal complex and a 4-coordinate, 8-electron main group alkyl compound,[13] one can say that d^0 Cp_2MR_2 ⫟ AlR_3 and d^0 Cp_2MR ⫟ MgR_2 ⫟ ZnR_2. Equation 2 can then be varied by substituting the d^0 ML_n moiety by, for example, $AlEt_3$, $MgEt_2$, or $ZnEt_2$.

Appendix

The calculations have been carried out within the extended Hückel formalism,[14] using the weighted H_{ij} formula.[15] The atomic

Table I. Parameters Used in Extended Hückel Calculations[a]

orbital		H_{ii}, eV	ξ_1	ξ_2	C_1[a]	C_2[a]
H	1s	−13.6	1.30			
C	2s	−21.4	1.625			
		−11.4	1.625			
Lu	6s	−6.05	1.666			
	6p	−6.05	1.666			
	5d	−5.22	2.813	1.210	0.7044	0.4880
	4f	−12.40	9.136	3.666	0.7330	0.4459
Sm	6s	−4.86	1.400			
	6p	−4.86	1.400			
	5d	−6.06	2.747	1.267	0.7184	0.4447
	4f	−11.28	6.907	2.639	0.7354	0.4597

[a] The d and f orbitals are formed by a linear combination of two simple Slater functions.

(9) Barefield, E. K.; Parshall, G. W.; Tebbe, F. N. *J. Am. Chem. Soc.* **1970**, *92*, 5224. Klabunde, U.; Parshall, G. W. *J. Am. Chem. Soc.* **1972**, *94*, 9081. Foust, D. F.; Rogers, R. D.; Raush, M. D.; Atwood, J. L.; *J. Am. Chem. Soc.* **1982**, *104*, 5646. Curtis, M. D.; Bell, L. G.; Butler, W. M. *Organometallics*, **1985**, *4*, 701.

(10) Bruce, M. I. *Angew, Chem., Int. Ed. Engl.* **1977**, *16*, 73.

(11) Fendrich, C. M.; Marks, T. J. *J. Am. Chem. Soc.* **1984**, *106*, 2214. Bruno, J. W.; Smith, G. M.; Marks, T. J.; Fair, G. K.; Schultz, A. J.; William, J. M. *J. Am. Chem. Soc.* **1986**, *108*, 40. Fendrick, C. M.; Marks, T. J. *J. Am. Chem. Soc.* **1986**, *108*, 425. For a related H-abstraction reaction on Cp_2LuR compounds see: Watson, P. L. *J. Am. Chem. Soc.* **1982**, *104*, 6471.

(12) Podall, H. E.; Petree, E.; Zictz, J. R. *J. Org.* Chem. **1959**, *24*, 1222.

(13) Hoffmann, R. *Angew. Chem. Int. Ed. Engl.* **1982**, *21*, 711.

parameters listed in Table I are taken from a previous work on $LnCp_2$ hydrides.[8b] Calculations on **6** and **7** have been carried out with and without inclusion of Lu 4f orbitals. As previously noted,[8b] these orbitals are only slightly perturbed by the ligand environment, always staying below the occupied π(Cp) levels. Thus, for computational time saving, they were not introduced in subsequent calculations.

When not specified in the text, the following bond distances (angstroms) and angles (deg) where used: Lu–H = 2.1; Lu–CH_3 = 2.6; Lu–C(Cp) = 2.85; C(Cp)–C(Cp) = 1.42; C–H = 1.09; Cp(centroid)–Lu–Cp(centroid) = 135; H–C–H = 109.47.

The variation of the total electronic energy of the considered systems during reactions 10, 11, 3, and 18 was obtained from an hypothetical reaction coordinate based on a linear transit between the geometries of the starting point and the assumed midpoint of the reaction followed by another linear transit between the midpoint and the final point of the reaction. In the starting and ending geometries, H–H and C–H distances of H_2 and CH_4 were, respectively, 0.74 and 1.09 Å and the following intermolecular contacts (angstroms) were considdered: Lu···H = 2.6; Lu···C = 3.05. A reasonable change in these distances does not affect significantly the general shape of the energy curve. The zero energy corresponds to the starting molecules at infinite separation in their stable conformation.

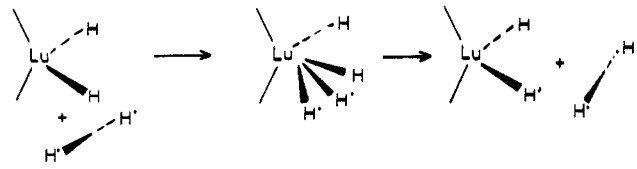

18

Acknowledgment. We thank Prof T. A. Albright for helpful discussions and Prof. T. J. Marks for providing results prior to publication.

(14) Hoffmann, R. *J. Chem. Phys.* **1963**, *39*, 1397. Hoffmann, R.; Lipscomb, W. N. *J. Chem. Phys.* **1962**, *36*, 2179; **1962**, *37*, 2872.
(15) Ammeter, J. H.; Bürgi, H.-B.; Thibeault, J. C.; Hoffmann, R. *J. Am. Chem. Soc.* **1978**, *100*, 3686.

Molecular Dynamics Simulation of a Small Calcium Complex in Aqueous Solution

Olle Teleman* and Peter Ahlström

Contribution from the Department of Physical Chemistry 2, Chemical Centre, University of Lund, POB 124, S-221 00 Lund, Sweden. *Received September 9, 1985*

Abstract: A molecular dynamics technique is used to simulate $CaEDTA^{2-}$ (two trajectories), H_4EDTA, and a calcium ion in aqueous solutions as well as pure water. The equation of motion is solved by means of a double time-step algorithm. The potential function allows for full intramolecular flexibility. The structure of "flexible" water resembles that of corresponding rigid water models, while dynamics seem slightly faster. This also applies to all dynamics of molecules dissolved in flexible water. The simulated coordination number of Ca^{2+} in a 0.45 M solution is 7. Comparison of the two $CaEDTA^{2-}$ trajectories indicates that quasiergodicity has been reached. In $CaEDTA^{2-}$ the calcium coordination number is also $\approx$7. Ligandation of calcium to the carboxyl groups is very strong, while the nitrogen–calcium relation is weaker. The structure of H_4EDTA is looser than that of $CaEDTA^{2-}$. Rotational correlation times for H_4EDTA are about half those of $CaEDTA^{2-}$, and the diffusion coefficient of H_4EDTA is about twice that of $CaEDTA^{2-}$. Both display some internal motion. Structural properties are plausibly reproduced, while dynamics seem fast. Results are compared to experimental data and discussed with respect to the properties of the potential.

Binding of calcium ions to different ligands is an important process in nature, where calcium ions frequently act as intracellular transmittor substances.[1] Many calcium-binding proteins with varying functions and binding constants ($K = 10^3$–10^8) are known.[1] Some proteins, e.g., calmodulins[2] and troponins,[3] work as regulators and undergo considerable conformational change on calcium binding. They often display a strong cooperativity that increases their sensitivity to changes in the calcium concentration. In other proteins, e.g., α-lactalbumin, the calcium ion is virtually permanently bound and appears to be a strongly connective structural element. In all of these proteins the calcium ion binds preferably to oxygen atoms in different amino acid residues, above all aspartic and glutamic acid.[1] The mechanisms of different processes involved in calcium binding is thus of great interest to molecular biology.

One way to obtain a deeper insight into the binding of calcium ions in proteins is to use computer simulation techniques. Recently we have embarked on such a study of the protein parvalbumin.[4] Such simulations however become rather complicated and very time-consuming. To provide a basis for their interpretation we have studied four smaller systems, namely pure water, one calcium ion in water, $CaEDTA^{2-}$ in water, and H_4EDTA in water. Pure water and calcium in water were mainly test systems for the model and the multiple time-step algorithm.[5] Comparison to experiment is possible since a wealth of X-ray and neutron diffraction data is available on the solvation of calcium ions, giving coordination numbers[6,7] and mean residence times[6] for the hydration shell of a calcium ion in water.

The $CaEDTA^{2-}$ complex is suitable as a test system for calcium binding because experimental data on both structure and dynamics

(1) Levine, B. A.; Williams, R. J. P. In *Calcium and Cell Function*; Cheung, W. W., Ed., Academic Press: London, 1982; pp 1–38.
(2) Perry, S. V. *Biochem. Soc. Trans.* **1979**, *7*, 593–617.
(3) Klee, C. B.; Crouch, T. H.; Richman, P. G. *Ann. Rev. Biochem.* **1980**, *49*, 489–515.
(4) Teleman, O.; Ahlström, P.; Jönsson, B. *Biophys. J.* **1985**, *47*, 399a.
(5) Teleman, O.; Jönsson, B. *J. Comput. Chem.* **1986**, *7*, 58–66.
(6) Friedman, H. L. *Chem. Scr.* **1985**, *25*, 42–48.
(7) Probst, M. M.; Radnai, T.; Heinzinger, K.; Bopp, P.; Rode, B. M. *J. Phys. Chem.* **1985**, *89*, 753–759.

0002-7863/86/1508-4333$01.50/0